



**HAL**  
open science

## Angular Quasi-Phase-Matching in Periodically Poled Uniaxial and Biaxial Crystals

Yannick Petit, Alexandra Peña, Simon Joly, Dazhi Lu, Patricia Segonds, Benoît Boulanger

► **To cite this version:**

Yannick Petit, Alexandra Peña, Simon Joly, Dazhi Lu, Patricia Segonds, et al.. Angular Quasi-Phase-Matching in Periodically Poled Uniaxial and Biaxial Crystals. *Crystals*, 2022, 12 (7), pp.979. 10.3390/cryst12070979 . hal-03726163

**HAL Id: hal-03726163**

**<https://hal.science/hal-03726163>**

Submitted on 18 Jul 2022

**HAL** is a multi-disciplinary open access archive for the deposit and dissemination of scientific research documents, whether they are published or not. The documents may come from teaching and research institutions in France or abroad, or from public or private research centers.

L'archive ouverte pluridisciplinaire **HAL**, est destinée au dépôt et à la diffusion de documents scientifiques de niveau recherche, publiés ou non, émanant des établissements d'enseignement et de recherche français ou étrangers, des laboratoires publics ou privés.

Review

# Angular Quasi-Phase-Matching in Periodically Poled Uniaxial and Biaxial Crystals

Yannick Petit <sup>1,2,\*</sup> , Alexandra Peña <sup>3</sup> , Simon Joly <sup>4</sup>, Dazhi Lu <sup>3,5</sup> , Patricia Segonds <sup>3</sup>  and Benoît Boulanger <sup>3,\*</sup><sup>1</sup> Université de Bordeaux, CNRS, CEA, CELIA, UMR 5107, F-33405 Talence, France<sup>2</sup> Université de Bordeaux, CNRS, Bordeaux INP, ICMCB, UMR 5026, F-33608 Pessac, France<sup>3</sup> Université Grenoble Alpes, CNRS, Grenoble INP, Institut Néel, 38000 Grenoble, France; alexandra.pena@neel.cnrs.fr (A.P.); dazhi.lu@sdu.edu.cn (D.L.); patricia.segonds@neel.cnrs.fr (P.S.)<sup>4</sup> University of Bordeaux, CNRS, IMS, UMR 5218, F-33405 Talence, France; simon.joly@u-bordeaux.fr<sup>5</sup> State Key Lab of Crystal Materials, Shandong University, Jinan 250100, China

\* Correspondence: yannick.petit@u-bordeaux.fr (Y.P.); benoit.boulanger@neel.cnrs.fr (B.B.)

**Abstract:** This article deals with a general description of Angular Quasi-Phase-Matching (AQPM) in uniaxial and biaxial crystals for second-order nonlinear optical interactions. Such an exhaustive and generalized angular-dependent approach of AQPM reveals new directions of propagation with efficient parametric frequency conversion. These AQPM solutions are studied by depicting the corresponding topologies and associated symmetries. The theoretical overview is fully validated and illustrated by measurements. We clearly demonstrate the benefits of such a generalized approach, both in the case of two emblematic periodically poled (PP) crystals: 5%MgO-doped PPLiNbO<sub>3</sub> (5%MgO:PPLN) and Rb-doped PPKTiOPO<sub>4</sub> (PPRKTP). These developments should stimulate new potential applications in nonlinear frequency conversion.

**Keywords:** nonlinear optics; frequency conversion; quasi-phase-matching; periodically poled crystals; second-harmonic generation; optical parametric oscillators



**Citation:** Petit, Y.; Peña, A.; Joly, S.; Lu, D.; Segonds, P.; Boulanger, B. Angular Quasi-Phase-Matching in Periodically Poled Uniaxial and Biaxial Crystals. *Crystals* **2022**, *12*, 979. <https://doi.org/10.3390/cryst12070979>

Academic Editors: Chunhui Yang, Ning Ye and Haohai Yu

Received: 10 June 2022

Accepted: 7 July 2022

Published: 13 July 2022

**Publisher's Note:** MDPI stays neutral with regard to jurisdictional claims in published maps and institutional affiliations.



**Copyright:** © 2022 by the authors. Licensee MDPI, Basel, Switzerland. This article is an open access article distributed under the terms and conditions of the Creative Commons Attribution (CC BY) license (<https://creativecommons.org/licenses/by/4.0/>).

## 1. Introduction

Efficient parametric nonlinear optical interactions are usually achieved thanks to birefringence phase-matching (BPM) in anisotropic monolithic crystals [1–5] or quasi-phase-matching (QPM) in crystals where the sign of the coefficients of the second-order electric susceptibility tensor can be periodically reversed [2,6–10].

As the first periodically poled KTiOPO<sub>4</sub> (PPKTP) and LiNbO<sub>3</sub> (PPLN) crystals had very limited aperture sizes of about 500 μm, interacting beams could only propagate along a unique direction that is orthogonal to the inverted domains planes, providing QPM along the grating period only. Advances in the poling process have led to longer and larger samples, allowing us to shape these periodically poled crystals as cylinders with centimetric diameters but still with sub-millimetric depth [11,12]. Such a cylindrical shape provides the possibility of a continuous variation of the angle between the direction normal to the inverted domains planes and the input laser beams propagation axis, leading to a remarkable improvement in the continuity of the spectral tunability and the output beam quality [11,12]. Further progress led to a thickness perpendicularly to the grating vector reaching more than 5 mm both in 5%MgO-doped PPLiNbO<sub>3</sub> (5%MgO:PPLN) and Rb-doped PPKTiOPO<sub>4</sub> (PPRKTP) [13,14]. It provided access to any direction of propagation of the input beams in the crystal with respect to the grating vector by keeping a sufficiently long interaction length. We called such a configuration angular quasi-phase-matching (AQPM), which led to a first step in the generalization of the QPM concept [15]. We showed that AQPM is well described by a collinear configuration between the wave vectors of the three interacting waves [11,15]. We also performed calculations in the case of 5%MgO:PPLN, which belongs to the uniaxial optical class. These studies have shown that

AQPM can provide larger spectral tunability and acceptances than those of BPM or QPM along the grating vector [15]; exhaustive calculations of spectral and angular tolerances have enlightened the diversity of AQPM potentials [16]. Moreover, we performed the first experimental demonstrations of the existence of AQPM directions, which were carried out by studying a millimetric 5%MgO:PPLN crystal cut as a sphere [17]: these results confirmed the theoretical AQPM description proposed by references [11,15,16], and also led to the refinement of the Sellmeier equations of the crystal. We also proposed an exhaustive determination and classification of the AQPM directions in uniaxial periodically poled crystals, reporting up to 74 classes of solutions and thus illustrating the impressive richness of AQPM interactions [18]. AQPM Second-Harmonic Generation (SHG) in a 25°-rotated, x-cut PPLiTaO<sub>3</sub> has also been achieved [19]. More recently, we verified the AQPM theory in the case of the biaxial optical class by performing SHG measurements in a PPRKTP crystal cut as a sphere [20]. We used the same sample to introduce a negative order AQPM SHG [21].

In this paper, we provide a unified theoretical description of positive and negative orders AQPM using group theory. The spaces of AQPM directions are then described and analyzed, including polarization dependence, topology and associated symmetry aspects. Moreover, such a generalized AQPM approach is applied to 5%MgO:PPLN and PPRKTP, with accessible poling periodicities, in order to provide their potential interest.

## 2. Generalized AQPM

We consider three interacting waves at wavelengths  $\lambda_1$ ,  $\lambda_2$  and  $\lambda_3$  with collinear wave vectors  $\vec{k}_1$ ,  $\vec{k}_2$  and  $\vec{k}_3$ , respectively. As described in ref. [15], a periodically poled medium with a periodicity  $\Lambda$  is characterized by an effective periodicity  $\Lambda(\alpha)$  along the direction of propagation of the interaction, where  $\alpha$  is the angle between the propagation direction of the three interacting wave vectors and the normal direction to the poled domains, as shown in Figure 1a. Such an effective periodicity implies an effective grating vector  $\vec{k}_{\Lambda(\alpha)}$  along the corresponding direction of propagation. We proposed the following generalized AQPM vector relation, which asserts a double criterion to perform momentum conservation during the considered nonlinear frequency conversion processes, i.e.,

$$\vec{k}_3 - \vec{k}_1 - \vec{k}_2 \mp \vec{k}_{\Lambda(\alpha)} = 0. \quad (1)$$

We call these two AQPM conditions scheme-A AQPM for equation  $\vec{k}_3 - \vec{k}_1 - \vec{k}_2 - \vec{k}_{\Lambda(\alpha)} = 0$ , i.e., positive order AQPM, and scheme-B AQPM for  $\vec{k}_3 - \vec{k}_1 - \vec{k}_2 + \vec{k}_{\Lambda(\alpha)} = 0$ , i.e., negative order AQPM: these two relations are depicted in Figure 1b,c, respectively. scheme-A AQPM has already been introduced in ref. [15] and scheme-B AQPM in ref. [21].

Equation (1) can be reduced to a scalar relation along the direction of propagation of unit vector  $\vec{s}(\theta, \phi)$ , where the phase-mismatch between the nonlinear polarization and the incident interacting waves is  $\Delta k(\theta, \phi) = k_3 - k_1 - k_2$ . The corresponding coherence length of the interaction is  $l_c(\theta, \phi) = \frac{\pi}{|\Delta k(\theta, \phi)|}$ ; it is a positive quantity, as the effective periodicity  $\Lambda(\theta, \phi)$ . Then, AQPM interactions may occur with  $\Delta k(\theta, \phi) \cdot l_c(\theta, \phi) = +\pi$  when  $\Delta k(\theta, \phi) > 0$ , or  $\Delta k(\theta, \phi) \cdot l_c(\theta, \phi) = -\pi$  when  $\Delta k(\theta, \phi) < 0$ , knowing that  $\Lambda(\theta, \phi) = 2l_c(\theta, \phi) = \frac{2\pi}{|\Delta k(\theta, \phi)|}$ . The latter equation is thus a double condition that corresponds to scheme-A AQPM when  $\Lambda(\theta, \phi) = +\frac{2\pi}{\Delta k(\theta, \phi)}$  with  $\Delta k(\theta, \phi) > 0$ , and to scheme-B AQPM when  $\Lambda(\theta, \phi) = -\frac{2\pi}{\Delta k(\theta, \phi)}$  with  $\Delta k(\theta, \phi) < 0$ . As already defined in ref. [15,21], the domains are set orthogonal to the x-axis so that the effective periodicity is  $\Lambda(\theta, \phi) = \frac{\Lambda}{|\sin\theta\cos\phi|}$ , leading to the effective grating vector

$\vec{k}_{\Lambda(\theta,\phi)} = \frac{2\pi}{\Lambda(\theta,\phi)} \vec{s}(\theta,\phi)$ . In such a context, Equation (1) reduces to  $\Delta k(\theta,\phi) = \pm \frac{2\pi}{\Lambda(\theta,\phi)}$  in the  $\vec{s}(\theta,\phi)$  direction, i.e., to the following double scalar equation:

$$\frac{n_3(\theta,\phi)}{\lambda_3} - \frac{n_1(\theta,\phi)}{\lambda_1} - \frac{n_2(\theta,\phi)}{\lambda_2} \mp \frac{1}{\Lambda(\theta,\phi)} = 0, \tag{2}$$

where  $n_i(\theta,\phi)$  is the refractive index in the  $\vec{s}(\theta,\phi)$  direction associated with the interacting wavelength  $\lambda_i$ , with  $i = 1, 2, 3$ . In this scalar description, scheme-A and scheme-B AQPM conditions are described by  $\frac{n_3(\theta,\phi)}{\lambda_3} - \frac{n_1(\theta,\phi)}{\lambda_1} - \frac{n_2(\theta,\phi)}{\lambda_2} - \frac{1}{\Lambda(\theta,\phi)} = 0$  and  $\frac{n_3(\theta,\phi)}{\lambda_3} - \frac{n_1(\theta,\phi)}{\lambda_1} - \frac{n_2(\theta,\phi)}{\lambda_2} + \frac{1}{\Lambda(\theta,\phi)} = 0$ , respectively. It is important to notice that AQPM processes may be understood as a continuous evolution of the phase-mismatch from 0 to  $+\pi$  or to  $-\pi$  when the distance of propagation continuously evolves from 0 to  $l_c(\theta,\phi)$ . The phase-mismatch is then followed by a sudden phase shift of  $\pm\pi$  at the crossing propagation through a given poled domain to the next inverted one: this phase shift resets in phase the nonlinear polarization and the radiated field at the entrance of each inverted domain, for both APQM schemes A and B, as illustrated in Figure 2a,b, respectively.

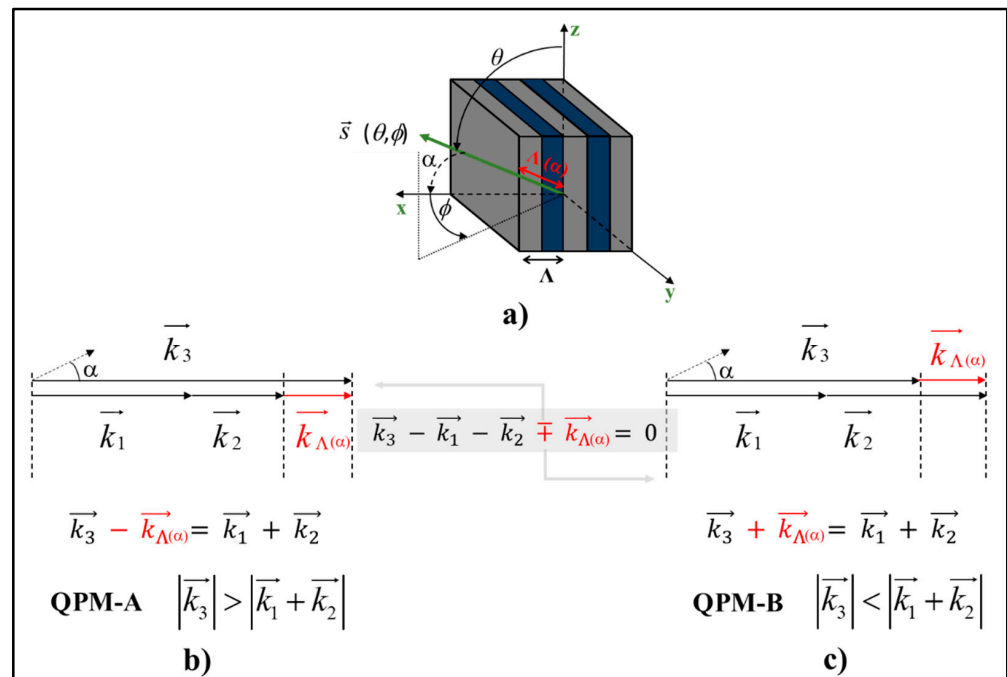


**Figure 1.** Collinear APQM configuration. (a) Scheme of the periodically poled medium with an inverting periodicity  $\Lambda$  and poled domain set to be orthogonal to the  $x$ -axis of the  $(x, y, z)$  dielectric frame of the medium.  $\vec{s}$  is the unit vector of the propagation direction of the three interacting waves;  $\theta$  and  $\phi$  are the angles of spherical coordinates of the propagation direction;  $\alpha$  is the angle between the unit vector of the propagation direction  $\vec{s}$  and the  $x$ -axis direction.  $k_{\Lambda(\alpha)}$  is the effective grating vector along the propagation direction;  $k_1, k_2$  and  $k_3$  are wave vectors of the interacting waves: (b) scheme-A APQM relation; (c) scheme-B APQM relation.

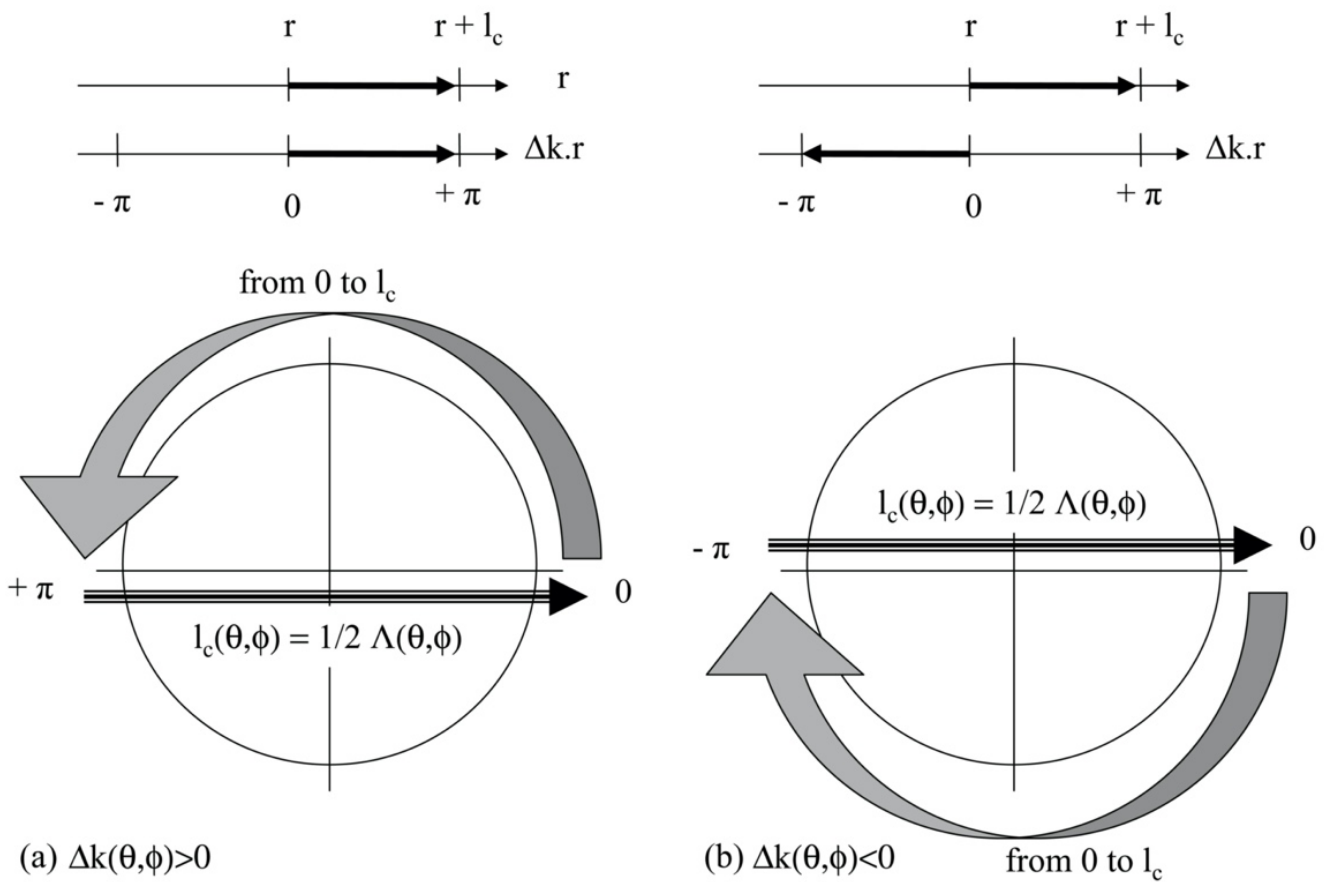


**Figure 2.** Phase mismatch evolution during a single sequence of AQPM with continuous evolution during continuous propagation along a single coherence length  $l_c$ , followed by a discontinuous phase reset at the immediate propagation from one domain to the next inverted one: (a) scheme-A AQPM; (b) scheme-B AQPM.

Note that BPM is included in both scheme-A and scheme-B AQPM conditions. Generalized AQPM conditions correspond to BPM when  $\Lambda(\theta, \phi) \rightarrow \infty$  in the  $yz$ -plane of the dielectric frame when the grating period is along the  $x$ -axis. Moreover, scheme-A and scheme-B AQPM tend to have the same single degenerated equation  $\Delta k(\theta, \phi) = \pm 0$  when  $\Lambda(\theta, \phi) \rightarrow \infty$ .

Equation (2) reveals the potential richness of generalized AQPM as it shows the combination of the angular tunability of the involved refractive indices and the effective periodicity with both  $\theta$  and  $\phi$  spherical angles.

From the corpuscular point of view, the AQPM condition  $\vec{\Delta k}_{AQPM} = \vec{\Delta k} - m\vec{k}_\Lambda = \vec{k}_3 - \vec{k}_1 - \vec{k}_2 - m\vec{k}_\Lambda = \vec{0}$ , with  $m = \pm 1$ , corresponds to momentum conservation between three photons and a quasi-particle depicting the periodically poled crystal through its grating vector  $\vec{k}_\Lambda$ , the latter bringing no energy. In the case  $m = 1$  (scheme-A), three particles with  $\vec{k}_1$ ,  $\vec{k}_2$  and  $\vec{k}_\Lambda$  are “consumed” to produce the new particle with the wave vector  $\vec{k}_3 = \vec{k}_1 + \vec{k}_2 + \vec{k}_\Lambda$ ; this is somehow equivalent to what occurs while considering Third-Harmonic Generation (THG) governed by the third-order electric susceptibility. Case  $m = -1$  (scheme-B) deals with two particles  $\vec{k}_1$  and  $\vec{k}_2$  that are “consumed” to produce a new pair of particles, one being the new photon associated with  $\vec{k}_3$  and the other one being the energy-less quasi-particle bearing the momentum quantum  $\vec{k}_\Lambda$  transferred to

the grating, with  $\vec{k}_3 + \vec{k}_\Lambda = \vec{k}_1 + \vec{k}_2$ ; this is similar to another four-particle interaction corresponding to Four-Wave Mixing (FWM) [21].

### 3. Polarization Configurations and Effective Coefficient

Due to the usual normal dispersion of the refractive indices with wavelength, i.e.,  $\frac{\partial n_i}{\partial \lambda_i} < 0$  [22], the phase-mismatch in the propagation direction  $\vec{s}(\theta, \phi)$  is positive, i.e.,  $\Delta k(\theta, \phi) = +\frac{2\pi}{\Lambda}(\theta, \phi) > 0$ , in the case of scheme-A AQPM, as seen above. However, the angular dependence of the grating term  $\frac{1}{\Lambda}(\theta, \phi)$  can afford AQPM solutions for Equation (2) for any of the  $2^3$  possible polarization configurations of the three interacting waves: indeed, for each propagating wavelength  $\lambda_i$ , there are two possible refractive indices  $n_i^+(\theta, \phi)$  and  $n_i^-(\theta, \phi)$ , with  $n_i^+(\theta, \phi) > n_i^-(\theta, \phi)$ . Then, the eight types are: I  $\{n_3^-, n_1^+, n_2^+\}$ , II  $\{n_3^-, n_1^-, n_2^+\}$ , III  $\{n_3^-, n_1^+, n_2^-\}$ , IV  $\{n_3^-, n_1^-, n_2^-\}$ , V  $\{n_3^+, n_1^+, n_2^+\}$ , VI  $\{n_3^+, n_1^-, n_2^+\}$ , VII  $\{n_3^+, n_1^+, n_2^-\}$  and VIII  $\{n_3^+, n_1^-, n_2^-\}$  [15]. Note that types II and III are equivalent in the case of SHG, which is the same for types VI and VII. In the BPM case, the solutions are limited to types I, II and III [3]. In the case of scheme-B AQPM, the phase-mismatch along  $\vec{s}(\theta, \phi)$  is negative, i.e.,  $\Delta k(\theta, \phi) = -\frac{2\pi}{\Lambda}(\theta, \phi) < 0$ . Due to a continuous spectral dispersion of the refractive indices  $n_i^\pm$ , and the continuous angular dependence of both the refractive indices and the effective grating periodicity, the phase-mismatch  $\Delta k(\theta, \phi)$  necessarily presents a continuous spectral and angular dependence. Therefore, the existence of BPM solutions implies the existence of negative values for  $\Delta k(\theta, \phi)$ , which is a necessary and sufficient condition to have access to scheme-B AQPM solutions of Equation (2). This implies that scheme-B AQPM is restricted to the three types that are also accessible under BPM conditions, i.e., types I, II and III. It appears here that scheme-B AQPM does not increase the number of possible types, nor does it enlarge the spectral tunability of solutions with respect to BPM solutions. However, the interest of scheme-B AQPM is that such a scheme provides new AQPM directions, which can enlarge the angular tunability of AQPM.

The efficiency of the eight types of generalized AQPM interactions presents angular and spectral dependences, but it also depends on the involved effective coefficient  $\chi_{eff}^{AQPM} = \chi^{(2)} \bullet (\vec{e}_3 \otimes \vec{e}_1 \otimes \vec{e}_2)$  [23]. Here,  $\vec{e}_1$ ,  $\vec{e}_2$  and  $\vec{e}_3$  are the unit field vectors of the three interacting waves;  $\chi^{(2)}$  is the second-order electric susceptibility tensor described by a matrix with 27 elements;  $\bullet$  and  $\otimes$  stand for contracted and tensorial products, respectively. The general expressions of the effective coefficient of SHG corresponding to the different types are provided in Table 1 for the crystal class  $3m$  and the negative uniaxial optical class, which corresponds to the case of 5%MgO:PPLN: the extraordinary (e) and ordinary (o) principal refractive indices verify  $n_e < n_o$ . Tables 2–4 concern the crystal class  $mm2$  and the positive biaxial optical class, which is the case of PPRKTP: the principal refractive indices verify  $n_x < n_y < n_z$ . In both cases, we applied symmetry due to the equality between two frequencies in SHG, i.e.,  $\chi_{ijk}(2\omega = \omega + \omega) = \chi_{ikj}(2\omega = \omega + \omega)$  [23].

Note that type IV is extensively used for propagation along the  $x$ -axis, i.e., along the grating vector, for both 5%MgO:PPLN and PPRKTP since, in that case, the effective coefficient depends on  $\chi_{zzz}$  only which magnitude is the highest [6,10–12,15]. However, as shown in the following, the effective coefficient is not the only parameter to consider. Actually, spectral acceptance can be of prime importance, especially in the case of the picosecond or femtosecond regimes. This point is discussed in more detail in Section 5.

**Table 1.** Effective coefficients of AQPM SHG corresponding to all possible configurations of polarization for AQPM SHG for the crystal class  $3m$  and the negative uniaxial optical class, which is the case of 5%MgO:PPLN. The  $\chi_{ijk}$  's stand for the independent coefficients of the second-order electric susceptibility tensor at  $2\omega$ .  $\rho_\omega$  and  $\rho_{2\omega}$  are the double refraction angles of the fundamental and second-harmonic waves, respectively. (o) and (e) stand for the ordinary and extraordinary polarizations, respectively.

Type ( $2\omega \ \omega \ \omega$ )	$\chi_{eff}^{(2)}$
I (e o o)	$\frac{2}{\pi} \{ \chi_{yyy} \cos(\theta + \rho_{2\omega}) \sin(\phi) [1 - 4\cos^2(\phi)] + \chi_{zxx} \sin(\theta + \rho_{2\omega}) \}$
II = III (e e o)	$\frac{2}{\pi} \chi_{yyy} \cos(\theta + \rho_{2\omega}) \cos(\theta + \rho_\omega) \cos(\phi) [4\sin^2(\phi) - 1]$
IV (e e e)	$\frac{2}{\pi} \left\{ \begin{array}{l} -\chi_{yyy} \cos(\theta + \rho_{2\omega}) \cos^2(\theta + \rho_\omega) \sin(\phi) [1 - 4\cos^2(\phi)] \\ + 2\chi_{xxz} \cos(\theta + \rho_{2\omega}) \sin(\theta + \rho_\omega) \cos(\theta + \rho_\omega) \\ + \sin(\theta + \rho_{2\omega}) [\chi_{zxx} \cos^2(\theta + \rho_\omega) + \chi_{zzz} \sin^2(\theta + \rho_\omega)] \end{array} \right\}$
V (o o o)	$\frac{2}{\pi} \chi_{yyy} \cos(\phi) [1 - 4\sin^2(\phi)]$
VI = VII (o e o)	$\frac{2}{\pi} \{ \chi_{yyy} \cos(\theta + \rho_\omega) \sin(\phi) [1 - 4\cos^2(\phi)] + \chi_{zxx} \sin(\theta + \rho_\omega) \}$
VIII (o e e)	$\frac{2}{\pi} \chi_{yyy} \cos^2(\theta + \rho_\omega) \cos(\phi) [4\sin^2(\phi) - 1]$

**Table 2.** Effective coefficient of AQPM SHG corresponding to all possible configurations of polarization for AQPM SHG in the yz-plane of the crystal class  $mm2$  and the positive biaxial optical class, which is the case of PPRKTP. The  $\chi_{ijk}$  's stand for the independent coefficients of the second-order electric susceptibility tensor at  $2\omega$ .  $\rho_\omega$  and  $\rho_{2\omega}$  are the double refraction angles of the fundamental and second-harmonic waves, respectively. (o) and (e) stand for the ordinary and extraordinary polarizations, respectively.

Type ( $2\omega \ \omega \ \omega$ )	yz-Plane $\chi_{eff}^{(2)}$
I (o e e)	0
II = III (o o e)	$\frac{2}{\pi} \chi_{xxz} \sin(\theta - \rho_\omega)$
IV (o o o)	0
V (e e e)	$\frac{2}{\pi} \left[ \begin{array}{l} 2\chi_{yyz} \cos(\theta - \rho_{2\omega}) \cos(\theta - \rho_\omega) \sin(\theta - \rho_\omega) \\ + \sin(\theta - \rho_{2\omega}) (\chi_{zyy} \cos^2(\theta - \rho_\omega) + \chi_{zzz} \sin^2(\theta - \rho_\omega)) \end{array} \right]$
VI = VII (e o e)	0
VIII (e o o)	$\frac{2}{\pi} \chi_{zxx} \sin(\theta - \rho_{2\omega})$

**Table 3.** Effective coefficient of AQPM SHG corresponding to all possible configurations of polarization for AQPM SHG in the xy-plane of the crystal class *mm2* and the positive biaxial optical class, which is the case of PPRKTP. The  $\chi_{ijk}$  's stand for the independent coefficients of the second-order electric susceptibility tensor at  $2\omega$ .  $\rho_\omega$  and  $\rho_{2\omega}$  are the double refraction angles of the fundamental and second-harmonic waves, respectively. (o) and (e) stand for the ordinary and extraordinary polarizations, respectively.

		xy-Plane
Type (2 $\omega$ $\omega$ $\omega$ )		$\chi_{eff}^{(2)}$
I (o e e)		0
II = III (o o e)	$\frac{2}{\pi} [\chi_{xxz} \sin(\phi - \rho_{2\omega}) \sin(\phi - \rho_\omega) + \chi_{yyz} \cos(\phi - \rho_{2\omega}) \cos(\phi - \rho_\omega)]$	
IV (o o o)		0
V (e e e)		$\frac{2}{\pi} \chi_{zzz}$
VI = VII (e o e)		0
VIII (e o o)	$\frac{2}{\pi} [\chi_{zxx} \sin^2(\phi - \rho_\omega) + \chi_{zyy} \cos^2(\phi - \rho_\omega)]$	

**Table 4.** Effective coefficient of AQPM SHG corresponding to all possible configurations of polarization for AQPM SHG in the xz-plane of the crystal class *mm2* and the positive biaxial optical class, which is the case of PPRKTP. The  $\chi_{ijk}$  's stand for the independent coefficients of the second-order electric susceptibility tensor at  $2\omega$ .  $\rho_\omega$  and  $\rho_{2\omega}$  are the double refraction angles of the fundamental and second-harmonic waves, respectively. (o) and (e) stand for the ordinary and extraordinary polarizations, respectively.  $V_z(\omega)$  and  $V_z(2\omega)$  are the optical axes at  $\omega$  and  $2\omega$ , respectively, with  $V_z(\omega) < V_z(2\omega)$  in the case of PPRKTP.

		xz-Plane
Type (2 $\omega$ $\omega$ $\omega$ )		$\chi_{eff}^{(2)}$
I (e o o) (o e e)	$0 < \theta < V_z(\omega)$ $V_z(2\omega) < \theta < 90^\circ$	$\frac{2}{\pi} \chi_{zyy} \sin(\theta - \rho_{2\omega})$ 0
II = III (e e o) (o o e)	$0 < \theta < V_z$ $V_z(2\omega) < \theta < 90^\circ$	0 $\frac{2}{\pi} \chi_{yyz} \sin(\theta - \rho_\omega)$
IV (e e e) (o o o)	$0 < \theta < V_z(\omega)$ $V_z(2\omega) < \theta < 90^\circ$	$\frac{2}{\pi} \left[ \begin{array}{l} 2\chi_{xxz} \cos(\theta - \rho_{2\omega}) \cos(\theta - \rho_\omega) \sin(\theta - \rho_\omega) \\ + \sin(\theta - \rho_{2\omega}) \left( \begin{array}{l} \chi_{zxx} \cos^2(\theta - \rho_\omega) + \\ \chi_{zzz} \sin^2(\theta - \rho_\omega) \end{array} \right) \end{array} \right]$
V (o o o) (e e e)	$0 < \theta < V_z(\omega)$ $V_z(2\omega) < \theta < 90^\circ$	$\frac{2}{\pi} \left[ \begin{array}{l} 0 \\ 2\chi_{xxz} \cos(\theta - \rho_{2\omega}) \cos(\theta - \rho_\omega) \sin(\theta - \rho_\omega) \\ + \sin(\theta - \rho_{2\omega}) \\ \left( \chi_{zxx} \cos^2(\theta - \rho_\omega) + \chi_{zzz} \sin^2(\theta - \rho_\omega) \right) \end{array} \right]$
VI = VII (o e o) (e o e)	$0 < \theta < V_z(\omega)$ $V_z(2\omega) < \theta < 90^\circ$	$\frac{2}{\pi} \chi_{yzy} \sin(\theta - \rho_\omega)$ 0
VIII (o e e) (e o o)	$0 < \theta < V_z(\omega)$ $V_z(2\omega) < \theta < 90^\circ$	0 $\frac{2}{\pi} \chi_{yyy} \sin(\theta - \rho_{2\omega})$

## 4. Symmetry and Topology Analyses

### 4.1. Symmetry Group Approach

We are interested in the symmetry groups  $G_{AQPM}$  of the space of solutions of scheme-A and scheme-B AQPM, i.e.,  $\vec{s}_A(\theta, \phi)$  and  $\vec{s}_B(\theta, \phi)$ . These groups can be built on the basis of the symmetry groups  $G_3, G_1, G_2$  and  $G_\Lambda$  of the four surfaces associated with the four parts of Equation (2):  $\frac{n_3(\theta, \phi)}{\lambda_3}, \frac{n_1(\theta, \phi)}{\lambda_1}, \frac{n_2(\theta, \phi)}{\lambda_2}$  and  $\frac{1}{\Lambda(\theta, \phi)}$ . Then, comes [15]:

$$G_{AQPM} = G_3 \cap G_1 \cap G_2 \cap G_\Lambda. \quad (3)$$

Group  $G_\Lambda$  corresponds to a finite closed surface that belongs to the infinite group of orientation symmetry of the cylinder with the axis of revolution along the  $x$ -axis [15,23], i.e.,  $G_\Lambda = G_{cylinder//x}$ . The angular distributions of the terms  $\frac{n_i(\theta, \phi)}{\lambda_i}$ , with  $i = 1, 2$  and  $3$ , are related to the index surface at the proper wavelength and the proper polarization, which thus requires to specify the optical class as described below.

In the case of periodically poled uniaxial crystals such as 5%MgO:PPLN [15], the index surface is composed of one ordinary layer and one extraordinary layer of principle refractive indices  $n_o$  and  $n_e$ , respectively [23]. Note that  $(n_e, n_o)$  correspond to  $(n^-, n^+)$  because 5%MgO:PPLN is a negative uniaxial crystal. The ordinary layer is a sphere of radius  $n_o(\theta, \phi) = n_o$ , which group of symmetry is  $G_{sphere}$ ; the extraordinary layer is an ellipsoid of revolution around the  $z$ -axis of equation  $n_e^{-2}(\theta, \phi) = \left(\frac{\cos\theta}{n_o}\right)^2 + \left(\frac{\sin\theta}{n_e}\right)^2$  that belongs to the group of the cylinder, as for the grating, but with the revolution axis along the  $z$ -axis, i.e.,  $G_{cylinder//z}$  [15,24]. Two situations can occur depending on the involved refractive index layers and associated type of interaction.

- The first case is that of type V, where the three interacting waves solicit the ordinary index layer so that the AQPM symmetry group restricts to  $G_{AQPM} = G_{sphere} \cap G_{cylinder//x} = G_{cylinder//x}$ .
- The second case deals with the seven other types that involve at least one polarization mode related to the extraordinary index layer, i.e., types I, II, III, IV, VI, VII and VIII. Here, the symmetry group  $G_{AQPM}$  is provided by  $G_{AQPM} = G_{cylinder//x} \cap G_{cylinder//z} = mmm$ , where  $mmm$  is the finite group of orientation symmetry of the orthorhombic system: it corresponds to the three mirrors  $m$  with respect to the three principal planes of the dielectric frame.

Finally, biaxial periodically poled media, such as PPRKTP, exhibit the  $mmm$  symmetry group for each refractive index layer of the index surface so that the associated symmetry group are always  $mmm$ . Thus, the resulting symmetry group associated with Equation (3) is always  $G_{AQPM} = mmm \cap G_{cylinder//x} = mmm$ , whatever the considered type among the  $2^3 = 8$  possible polarization combinations of the considered scheme A or B.

Note that for both uniaxial and biaxial periodically poled media, scheme-A AQPM applies for the eight possible types of interaction, with spaces of solutions  $\vec{s}_A(\theta, \phi)$  associated with the detailed groups of symmetry. As scheme-B AQPM is restricted to types I, II and III, spaces of solutions  $\vec{s}_B(\theta, \phi)$  are thus always restricted to the  $mmm$  symmetry group. Thus, when used simultaneously for a given type, both scheme-A and scheme-B AQPM spaces of solutions share the same symmetry group, as these two schemes share the same polarization configuration.

### 4.2. Topologies of Generalized AQPM

As already defined, spaces of AQPM solutions  $\vec{s}(\theta, \phi)$  correspond to the spherical angles  $(\theta, \phi)$  being solutions of Equation (1). These angular solutions can be depicted in Cartesian representation, such as curves  $\theta(\phi)$  (or  $\phi(\theta)$  equally). Alternatively, there is another suited representation known as the Wulff diagram, which corresponds to a stereographic projection of one octant of a sphere in a plane, as shown in Figure 3.

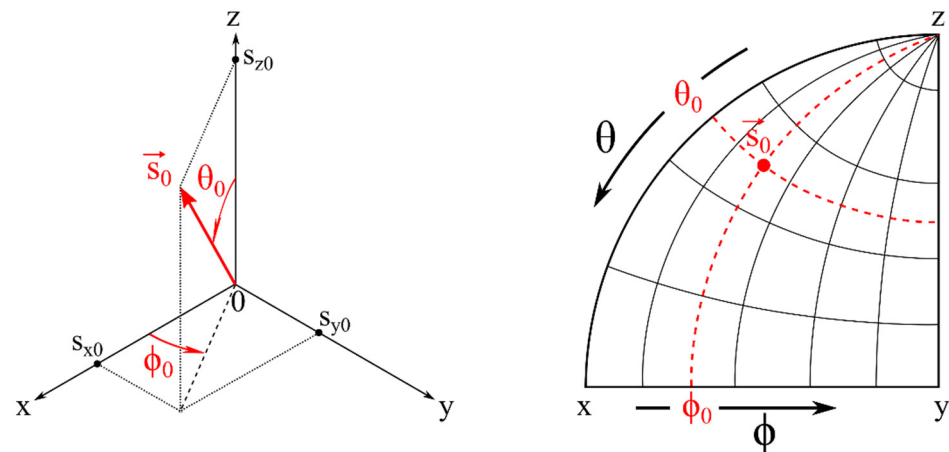


**Figure 3.** Wulff diagram (**right**) providing a useful planar representation of one octant (**left**) where boundaries correspond to the three principal planes of the dielectric frame.  $(O,x,y,z)$  is the dielectric frame and  $(\theta_0, \phi_0)$  are spherical angles of unit vector  $\vec{s}_0$  standing for any direction of propagation.

For a given set of wavelengths  $(\lambda_1, \lambda_2, \lambda_3)$ , the AQPM directions  $\vec{s}_{AQPM}(\theta, \phi)$  form cones of circular or non-circular contours that wrap around specific axes. Their topologies and orientations depend on the relations of order, regarding the wavelength dispersion and configuration of polarization, between the three quantities that constitute Equation (2), i.e.,  $\frac{n_3(\theta, \phi)}{\lambda_3}$ ,  $\left(\frac{n_1(\theta, \phi)}{\lambda_1} + \frac{n_2(\theta, \phi)}{\lambda_2}\right)$  and  $\mp \frac{1}{\Lambda(\theta, \phi)}$  as explained in [14,17] in the case of scheme-A for the uniaxial optical class.

There is no question here of repeating these explanations for scheme-A in uniaxial crystals. In summary, there are three possible winding directions as depicted in Figure 4: along the  $x$ -axis (topology  $T_x^A$ ), a given direction of the  $xz$ -plane (topology  $T_x^A$ ) and the  $z$ -axis (topology  $T_z^A$ ). The contours of the cone are generally not circular, except in the case where the three interacting waves are ordinary polarized, i.e., either for type IV in the case of positive uniaxial media or for type V according to Table 1 in the case of negative uniaxial media. In the latter negative uniaxial case, the cones belong to the group  $G_{cylinder//x}$ , while the symmetry is  $mmm$  for all the other cases since there is at least one extraordinary wave. Note that for BPM in uniaxial media, there is only one possible topology that corresponds to a circular cone oriented along the  $z$ -axis [3], as shown in Figure 4; the symmetry group is then  $G_{cylinder//z}$ .

The topology concerning scheme-B AQPM can be easily found without any calculation. It is indeed sufficient to consider the topological continuity between AQPM and BPM. Both scheme-A and scheme-B AQPM tend to BPM when the propagation occurs in the  $yz$ -plane of the periodically poled crystal since it corresponds to an infinite poling period  $\Lambda(\theta, \phi = \pi/2) \rightarrow \infty$ : then  $1/\Lambda \rightarrow 0$  in Equation (1), which corresponds to the BPM equation. Following this approach of continuity, it is clear that the types of the AQPM topologies  $T_z^A$  and  $T_z^B$  are those of BPM, i.e., types I, II and III. On the other hand, the two other AQPM topologies ( $T_x^A, T_{xz}^A$ ) can be relative to types IV, V, VI, VII or VIII, knowing that type IV, for positive uniaxial crystals, and type V, for the negative ones, are only associated with  $T_x^A$  as mentioned above.

In the case of periodically poled biaxial crystals such as PPRKTP, the concept of continuity shall further be invoked, from the uniaxial class to the biaxial class, on the one hand, and from BPM ( $\Lambda \rightarrow \infty$ ) to AQPM (finite period  $\Lambda$ ) solutions, on the other hand. It is then obvious that the AQPM topologies of the biaxial class contain the five possible ones of BPM that are reminded in Figure 5 [3], which contain themselves the AQPM topologies of the uniaxial class depicted in Figure 4.

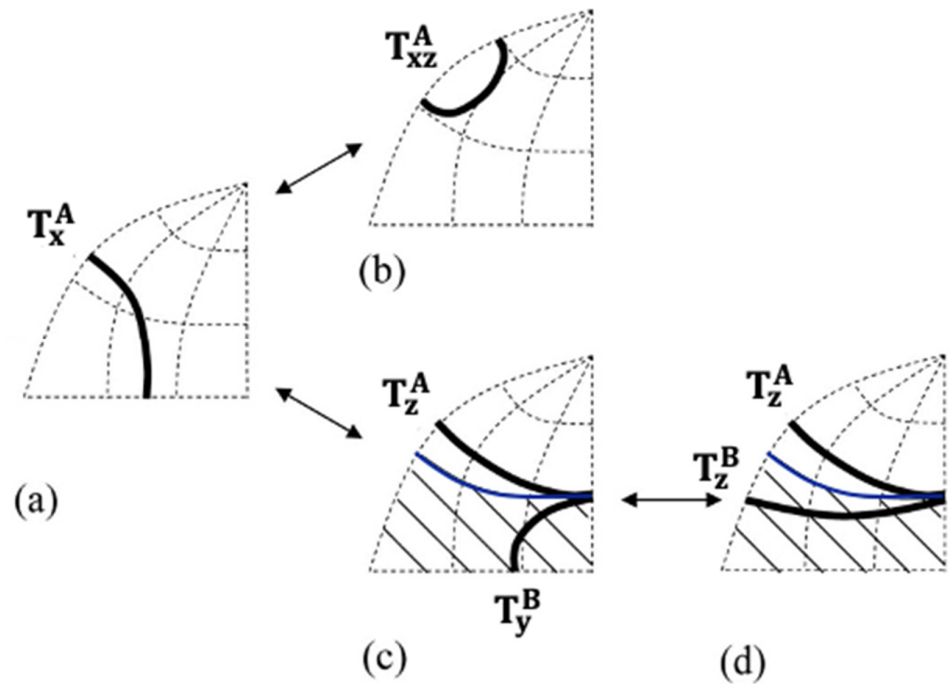


**Figure 4.** Topologies of scheme-A ( $\Delta k(\theta, \phi) > 0$ ) AQPM solutions ( $T_x^A, T_{xz}^A, T_z^A$ ) and scheme-B ( $\Delta k(\theta, \phi) < 0$ ) AQPM solutions ( $T_y^B, T_z^B$ ) in uniaxial periodically poled crystals. (a–d) Paths of continuous evolution with spectral dispersion of the AQPM solutions and associated topologies. The blue lines depict the circular cones of BPM ( $\Delta k(\theta, \phi) = 0$ ) solutions, which corresponds to boundaries between angular domains ( $\Delta k(\theta, \phi) > 0$ ) that are compatible with scheme-A AQPM and angular domains ( $\Delta k(\theta, \phi) < 0$ ) that are compatible with scheme-B AQPM.

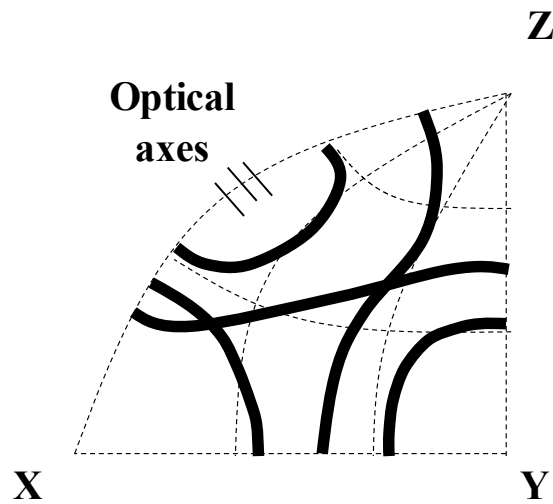


**Figure 5.** BPM Topologies of biaxial media, which are also possible topologies for AQPM. The three lines crossing the xz-plane stand for the optical axes at the wavelengths of the three interacting waves.

In the case of biaxial media, all these topologies are a priori compatible with both schemes-A AQPM and scheme-B AQPM. In fact, BPM ( $\Delta k(\theta, \phi) = 0$ ) solutions correspond to boundaries between angular domains that are compatible with scheme-A AQPM ( $\Delta k(\theta, \phi) > 0$ ) and angular domains compatible with scheme-B AQPM ( $\Delta k(\theta, \phi) < 0$ ).

## 5. Experimental Validation of the AQPM

### 5.1. Setups and Methods

The measurement of BPM, as well as AQPM directions, requires direct access to any direction of propagation in the dielectric frame of the considered material under study. The optimal methodology is to consider materials shaped as a sphere with its surface polished to optical quality [25,26]. Such a spherical sample needs to be oriented both from crystallographic and optical points of view by means of correlative X-ray diffraction and double refraction observation, respectively. Then, the full angular distribution of both linear and nonlinear optical properties can be addressed using only one sample of the studied sample by rotating the sphere within a high precision goniometric setup, which can be an Euler circle as well as a Kappa circle. In this way, it is possible to obtain direct access to the directions of propagation that correspond to solutions of BPM or AQPM interactions, whatever the considered type of polarization scheme or the involved set of wavelengths. Doing so allows us to propagate light along a diameter of the sphere by keeping normal incidence which is not possible while considering slab samples [25,26]. Figure 6a illustrate the scheme of an oriented periodically poled crystal. Figure 6b,c show the remarkable realization of millimetric-scale oriented periodically poled spherically shaped crystals of the uniaxial 5%MgO:PPLN [16–18] and of the biaxial PPRKTP [20,21], respectively.

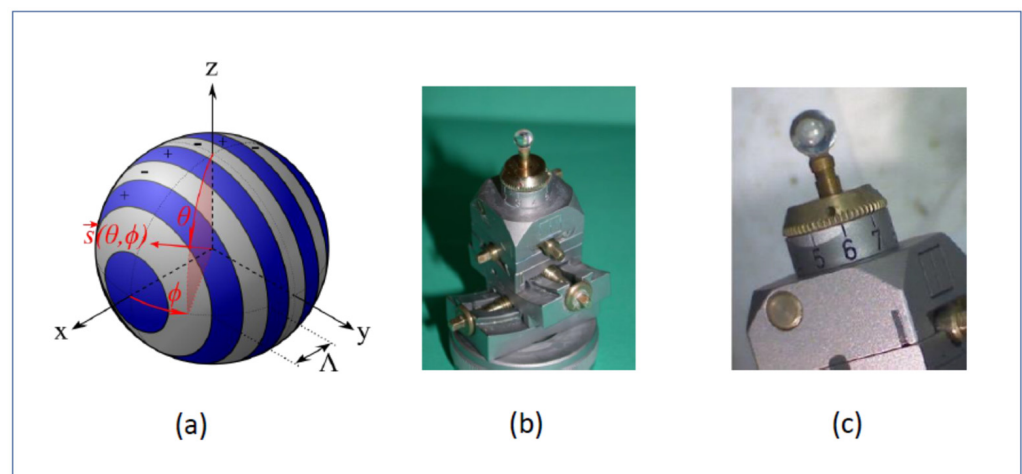


**Figure 6.** (a) Scheme of a periodically poled crystal oriented in the dielectric frame  $(x, y, z)$  where  $(\theta, \phi)$  are the spherical angle coordinates of the direction  $\vec{s}$ ; (b) 5%MgO:PPLN sphere with a grating period  $\Lambda = 32 \mu\text{m}$  and a diameter of 3.9 mm; (c) PPRKTP sphere with a grating period  $\Lambda = 38.52 \mu\text{m}$  and a diameter of 4.76 mm.

The diameter of the sphere is determined by the volume of the initial parallelepipedal sample, knowing that we try to obtain the biggest diameter as possible in order to access a minimal asphericity, typically better than 1% [26]. A spherically shaped sample provides the full metrological potentiality for the complete characterization of nonlinear materials. Indeed, such geometry allows for direct three-directional access out of the dielectric planes so that it is possible to determine cones of BPM as well as both scheme-A AQPM and scheme-B AQPM solutions with an angle accuracy of  $\pm 0.5^\circ$ . This also leads to a direct determination of the relative signs and absolute magnitude of the nonlinear coefficients, with a typical relative accuracy of  $\pm 10\%$ , by measuring the evolution of the effective coefficient along the cone [27]. It is also possible to access the spectral and angle acceptances of any BPM or AQPM direction. All these aspects will be specifically detailed hereafter in Section 5.2 in the case of Second-Harmonic Generation (SHG). Note that for applicative aspects, it is generally sufficient to access directions in only one single dielectric plane that gives access to the best effective coefficient or to the optimal acceptances. Then, the periodically poled crystal can be shaped as oriented cylinders, which is of great interest

because this geometry provides an infinite angle tunability than usual parallelepiped-shaped samples. The cylindrical geometry has major importance for Optical Parametric Oscillators (OPO), as further detailed in Section 5.3.

### 5.2. Experimental Demonstrations of AQPM SHG

The simplest demonstration of AQPM theory and associated solutions from Equation (2) comes from SHG experiments. AQPM SHG directions were investigated in a negative uniaxial 5% MgO:PPLN shaped as a sphere with a diameter of 3.9 mm. The nonlinear grating was oriented with domains perpendicular to the  $x$ -axis, similarly to the configuration described in Section 4, with a nonlinear period  $\Lambda = 32.2 \mu\text{m}$  and a 50% duty cycle ratio defined as the proportion of inverted domains with the same dimension. As shown in Figure 7a, type I SHG AQPM tuning curves were recorded with respect to the fundamental wavelength, either in the  $xz$ -plane ( $\phi = 0^\circ$ ) or in the  $yz$ -plane ( $\phi = 90^\circ$ ), the latter corresponding also to BPM solutions, as the effective period  $\frac{1}{\Lambda(\theta, \phi=90^\circ)} \rightarrow 0$  in the  $yz$ -plane.

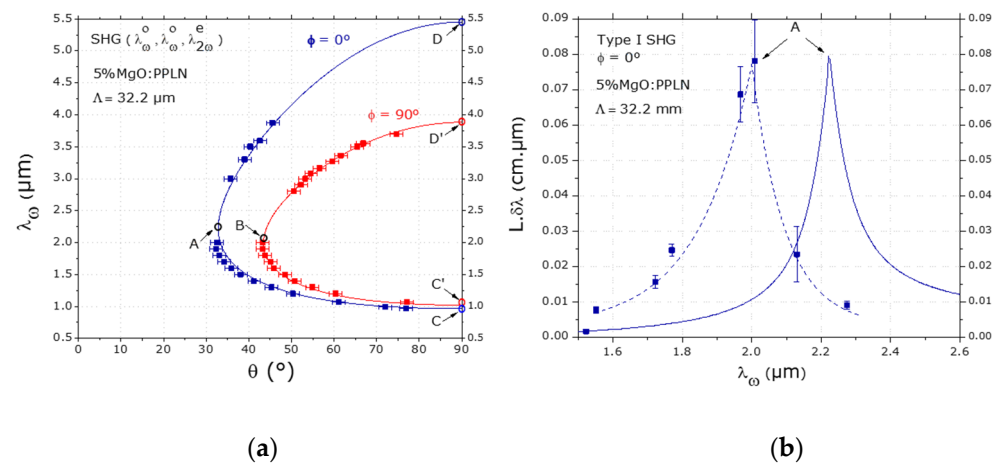


**Figure 7.** (a) Type I ( $eo0$ ) SHG AQPM tuning curves of 5%MgO:PPLN; the fundamental wavelength  $\lambda_\omega$  is given as a function of  $\theta$  at  $\phi = 0^\circ$  and  $\phi = 90^\circ$ . (o) and (e) denote the ordinary and extraordinary polarizations, respectively. Dots stand for experimental data, and solid curves are the fits [17]. Vertical tangents of the curves at points A and B correspond to spectrally noncritical interactions. Points C, C', D and D' are both BPM and AQPM directions since the grating has an infinite period  $\phi = 90^\circ$ . (b) Type I SHG AQPM spectral acceptances in the  $xy$ -plane as a function of the fundamental wavelength  $\lambda_\omega$ . Dots stand for experimental data; the dotted curve is a guide for the eyes, and the solid curve corresponds to calculations from Sellmeier equations given in [17]. The maximum denoted A, corresponds to the vertical tangent of the curve of (a).

The demonstration is instructive in various aspects. From a fundamental point of view, AQPM solutions extend the spectral range for SHG solutions as new fundamental wavelengths can be frequency-doubled such as those in the range between dots C and C', but also between points D' and D. Figure 7a also show the ability to continuously tune the spectral position of noncritical angle acceptances in the mid-IR, by sweeping planes at iso- $\phi$  angles, from the BPM solution (point D' corresponding to the  $y$ -axis, i.e.,  $\theta = 90^\circ$  and  $\phi = 90^\circ$ ) to the AQPM solution (point D corresponding to the  $x$ -axis, i.e.,  $\theta = 90^\circ$ ,  $\phi = 0^\circ$ ). The fundamental wavelength ranging between D and D' can also be addressed in the  $xz$ -plane by adjusting the  $\phi$  angle. Moreover, the spectral acceptance can also reach a maximal amplitude, up to almost 78 nm.cm, at a wavelength for which the AQPM curve exhibits a vertical tangent, i.e., points A and B in Figure 7a.

The nonlinear effective coefficient is of importance for AQPM, as is the case for BPM. Of course, the largest accessible nonlinear coefficient remains  $\chi_{zzz}^{(2)}$ , such as usually addressed in most of the literature while disregarding any angular dependence. Still, as illustrated

in Figure 7b, where giant spectral acceptances appear, a tread-off between the effective coefficient and the spectral acceptance can be relevant in specific cases. Indeed, the effective coefficient has an angular distribution that is associated with each type of polarization set, whatever the considered scheme: BPM, scheme-A and scheme-B AQPM. This is illustrated in Figure 8, corresponding to calculations relative to SHG at a fundamental wavelength  $\lambda_\omega$  of 1550 nm in 5%MgO:PPLN with a grating period  $\Lambda = 32 \mu\text{m}$ , which is interesting in the context of telecommunications or for eye-safe security issues. Both BPM, scheme-A and scheme-B cones exhibit the same topology, from the xz-plane to the yz-plane, with a degenerated solution in the yz-plane, as shown in Figure 8a.

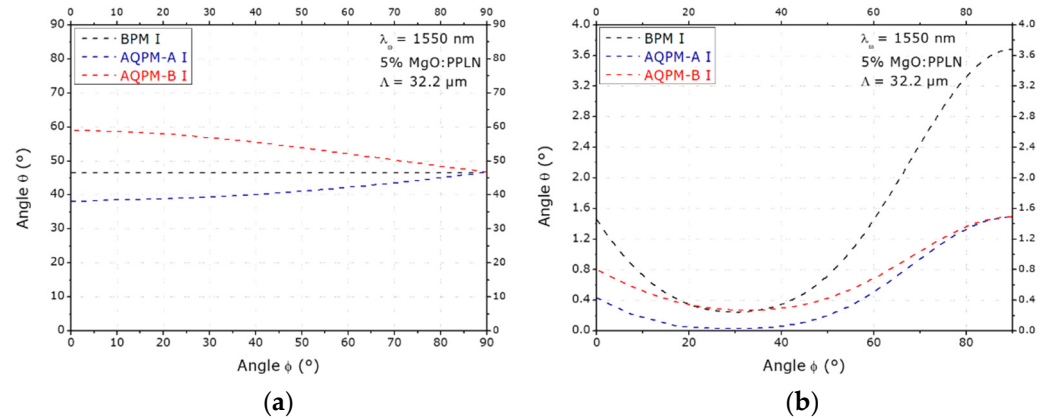


**Figure 8.** Comparison between AQPM and BPM solutions in the case of a type I SHG interaction at fundamental wavelength  $\lambda_\omega = 1550 \text{ nm}$  in 5%MgO:PPLN with a poling periodicity  $\Lambda = 32.2 \mu\text{m}$ : (a) AQPM directions of scheme-A (blue dashed line), scheme-B (red dashed line) and BPM solutions (black dashed line); (b) Corresponding Figures of Merit.

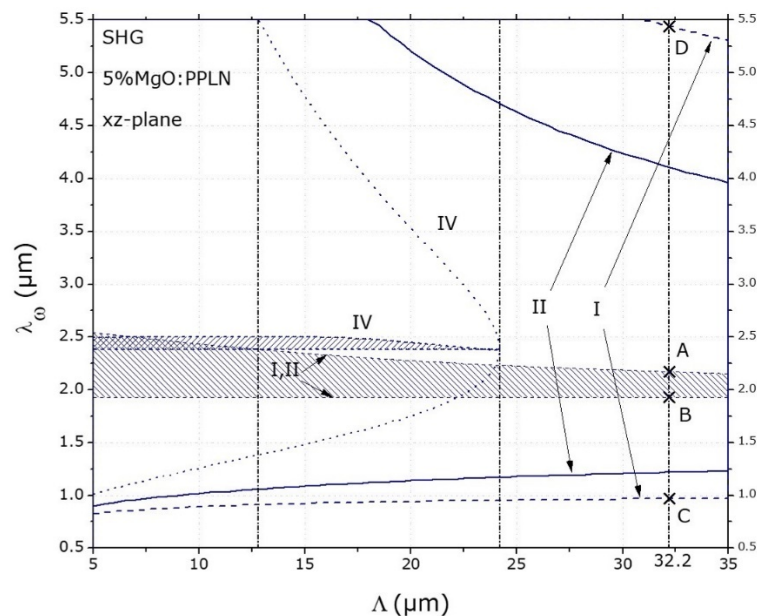
As a consequence, the different solutions of directions,  $(\theta_A, \phi_A)$  for scheme-A AQPM and  $(\theta_B, \phi_B)$  for scheme-B AQPM, may lead to different values of the effective coefficients  $\chi_{eff}^A(\theta_A, \phi_A)$  and  $\chi_{eff}^B(\theta_B, \phi_B)$ , thus to different figures of merit,  $[\chi_{eff}^A(\theta, \phi)]^2 / [n_3^-(\theta_A, \phi_A)n_1^+(\theta_A, \phi_A)n_2^+(\theta_A, \phi_A)]$  and  $[\chi_{eff}^B(\theta, \phi)]^2 / [n_3^-(\theta_B, \phi_B)n_1^+(\theta_B, \phi_B)n_2^+(\theta_B, \phi_B)]$  as depicted in Figure 8b. We can note that the figure of merit of scheme-B AQPM appears, in this case, to be larger than that of scheme-A AQPM. These aspects strengthen the potential interest of scheme-B AQPM solutions with respect to scheme-A AQPM, which should be considered to optimally design devices for nonlinear parametric frequency conversion. Note that the AQPM figure of merit is, of course, attenuated by the Fourier  $4/\pi^2$  parameter compared to that of BPM [6].

Figure 9 provide the description of accessible types of SHG interactions in a 7%MgO:PPLN with a grating period  $\Lambda = 15 \mu\text{m}$ , showing the associated spectral ranges of solutions for BPM and for AQPM (left and right parts of Figure 9, respectively). Figure 9 clearly illustrate the enlargement of the spectral range that can undergo SHG while considering AQPM with respect to BPM, both for smaller and larger fundamental wavelengths, respectively, from 905 to 1050 nm and from 3400 to 5400 nm, compared to the 1050–3400 nm spectral range of BPM. Note that the SHG spectral range of scheme-B AQPM is the same as that of BPM but shows different directions of solutions and thus exhibits different effective coefficients. More specifically, the topology of the scheme-B type I SHG cone for a nonlinear period  $\Lambda = 15 \mu\text{m}$  corresponds to the  $T_y^B$  topology, while the  $T_z^B$  topology is observed for a nonlinear period  $\Lambda = 32.2 \mu\text{m}$  for the same scheme-B type I SHG cone, as seen in Figure 7a.

Types ( $\lambda_{2\omega} \lambda_{\omega} \lambda_{\omega}$ )	BPM		AQPM	
	$\lambda_{\omega}$ range	Topology	$\lambda_{\omega}$ range	Topology
I (e o o)	1050-3400 nm		905 - 1050 nm 1050 - 3400 nm 3400 - 5400 nm	
II = III (e e o)	X	X	1075 - 5400 nm	
IV (e e e)	∅	∅	1400 - 5400 nm	
V (o o o)	∅	∅	1510 - 5400 nm	
VI = VII (o e o)	∅	∅	2490 - 4640 nm	
VIII (o e e)	∅	∅	X	X

**Figure 9.** Comparison between the spectral ranges of BPM and AQPM topologies in 7%MgO:PPLN with a grating period of  $\Lambda = 15 \mu\text{m}$ . The black cones correspond to scheme-A and the red one to scheme-B. (o) and (e) denote the ordinary and extraordinary polarizations, respectively.  $\lambda_{\omega}$  and  $\lambda_{2\omega}$  are the fundamental and second-harmonic wavelengths, respectively. X means that there are no BPM or AQPM solutions using the wavelength dispersion equations of the refractive indices of 7%MgO:PPLN in Ref. [28]. The symbol  $\emptyset$  means that BPM types are not allowed.

As already discussed in Figures 8 and 9, the grating period has a major influence on both the spectral ranges and the directions of AQPM solutions for each type. Figure 10 highlight this influence: it depicts the fundamental wavelength tuning ranges and maximal acceptance domains of types I, II = III, and IV scheme-A AQPM SHG calculated in the xz-plane as a function of the grating periodicity  $\Lambda$ .



**Figure 10.** Fundamental wavelength tuning ranges (solid curves) and maximal acceptance domains (hatched zones) of types I, II, and IV AQPM SHG calculated in the xz-plane as a function of the grating periodicity  $\Lambda$ . Points A, B, C, and D refer to the points appearing on the tuning curves of Figure 7a.

AQPM in biaxial periodically poled crystals has been demonstrated in a PPRKTP sample shaped as a sphere with a diameter of 4.76 mm and a grating period of 38.52  $\mu\text{m}$ . SHG was investigated at a fundamental wavelength of 2.15  $\mu\text{m}$  by angularly following the cones of the accessible types, as shown in Figure 10.

BPM was characterized for both types I and II = III. Scheme-A showed experimental and numerical solutions for both types I, II = III, IV and V. Scheme-B solutions have also been determined, especially with the pioneer experimental demonstration for type II, as highlighted by the red stars in Figure 11 [20,21]. Both scheme-A and scheme-B AQPM solutions have shown the expected continuity with BPM solutions in the yz-plane ( $\phi = 90^\circ$ ) for types I and II = III. In the same manner, as evocated in Section 5.2, it is noticeable here that the topology of the scheme-B AQPM cone, i.e., connecting the xy-plane and yz-plane, differs from both the BPM and scheme-A AQPM cones connecting the xz-plane and yz-plane. Such results strengthen the importance of having a deep knowledge of the possible spaces of solutions, similarly to what was described in Section 4, in order to prevent missing some allowed interactions in some planes, both numerically or experimentally.

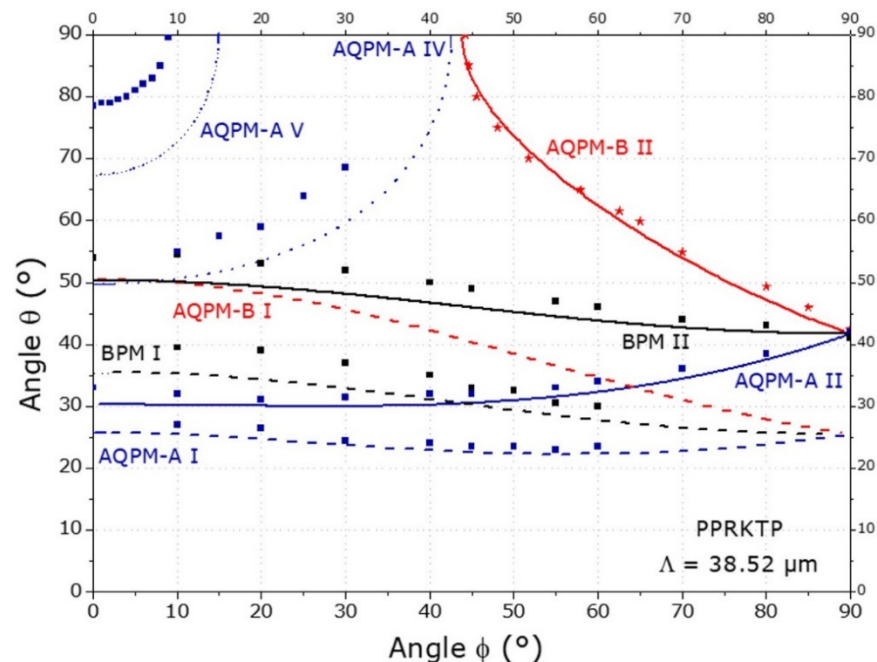


**Figure 11.** SHG at a fundamental wavelength  $\lambda\omega = 2.15 \mu\text{m}$  in a spherical PPRKTP crystal with a grating period  $\Lambda = 38.52 \mu\text{m}$ : calculated Types I and II BPM angles (black lines), calculated Types I, II, IV and V AQPM-A angles (blue lines), Types I and II AQPM-B angles (red lines) and red stars for the measurements described in [21]). Black and blue squares are experimental data obtained in [20].  $\theta$  and  $\phi$  are the angles of spherical coordinate in the dielectric frame ( $x, y, z$ ).

To go further with the demonstration of AQPM potentialities in biaxial crystals, numerical investigations have been conducted in PPRKTP with a grating period of 38.52  $\mu\text{m}$  for an SHG interaction in the xy-plane, using the Sellmeier equations given in [20]. As shown in Figure 12(top), the angular range as a function of the fundamental wavelength is reported for Type II solutions, both for BPM, scheme-A and scheme-B AQPM, as well as for Type V scheme-A AQPM solutions [21].

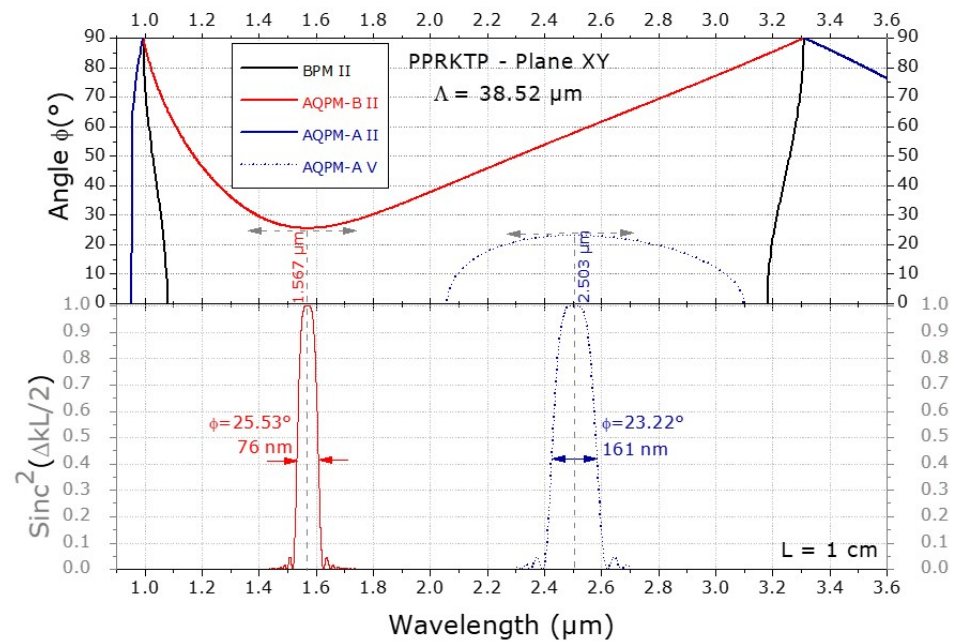


**Figure 12.** (Top) AQPM angle  $\phi$  versus fundamental wavelength  $\lambda\omega$  for SHG in the xy-plane of the PPRKTP with the poling period  $\Lambda = 38.52 \mu\text{m}$ : Type II BPM (full blackline); Type II AQPM-A and Type II AQPM-B (blue and red lines, respectively); Type V AQPM-A (grey dashed line). (Bottom) Spectral dependence of the  $\text{sinc}^2(\Delta kL/2)$  interference function for a crystal length  $L = 1 \text{ cm}$  under the Undepleted Pump Approximation (UPA) and at the spectral noncritical wavelengths  $\lambda\omega = 1.657 \mu\text{m}$  for Type II AQPM-B SHG (blue line) and  $\lambda\omega = 2.503 \mu\text{m}$  for Type V AQPM-A (red line).

Beyond the fact that the spectral range in the xy-plane differs from one type to another and from one scheme to another, it is worth noting that scheme-B type II and scheme-A type V present horizontal tangents at distinct fundamental wavelengths, thus exhibiting giant spectral tolerances at  $1.567 \mu\text{m}$  and  $2.503 \mu\text{m}$ , respectively. Scheme-B type II interaction thus opens broadband solutions of interest in the remarkable range of telecom wavelengths. The associated spectral acceptances (full width at 0.405 of the maximum) are estimated to be  $76 \text{ nm}$  for Scheme-B type II and even up to  $161 \text{ nm}$  for type V scheme-A. These extremely large values are, in many cases, more than two orders of magnitude larger than usual values, as shown in Figure 12(bottom) [21]. These results offer a clear illustration of the complementarity of the complete AQPM solutions with respect to the usual configuration that solicits the largest nonlinear coefficient  $\chi_{zzz}^{(2)}$ .

### 5.3. Experimental Demonstrations of AQPM OPO

AQPM can also be implemented in the configuration of OPO, which had been carried out in the case of PPKTP with a grating period  $\Lambda = 35 \mu\text{m}$  [29] and 5%MgO:PPLN with a grating period  $\Lambda = 28 \mu\text{m}$  [30].

In both cases, the configuration of polarization enabling the excitation of the largest nonlinear coefficient has been chosen, i.e.,  $\chi_{zzz}^{(2)}$  corresponding to  $2.d_{33}$  in the contracted notation: they refer to type V in the case of PPKTP according to Tables 2–4 and type IV for 5%MgO:PPLN according to Table 1. A cylindrical shape had been chosen for the two crystals, with a diameter of  $10 \text{ mm}$  for PPKTP and  $38 \text{ mm}$  for 5%MgO:PPLN, since only one dielectric plane allows us to access the full angular tunability, i.e., the xy-plane. Figure 13 depict the scheme of the corresponding experimental setup.

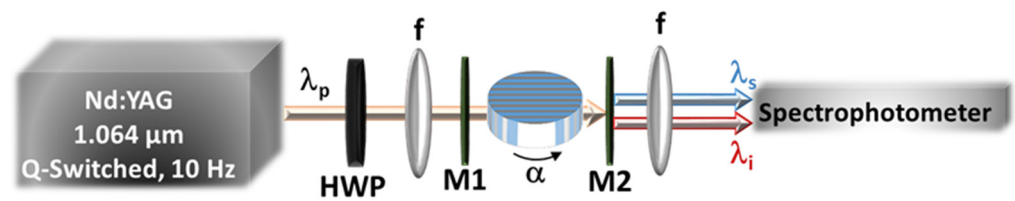


**Figure 13.** Experimental scheme of a cylindrical OPO. HWP is a half-wave plate. M1 and M2 are the two plane mirrors of the cavity. ( $\lambda_p$ ,  $\lambda_s$ ,  $\lambda_i$ ) are the pump, signal and idler wavelengths, respectively, verifying  $1/\lambda_p = 1/\lambda_s + 1/\lambda_i$ .

In both cases, it was a Singly Resonant OPO (SROPO) on the signal wavelength  $\lambda_s$ . The pump laser is a Q-switched Nd:YAG laser at  $\lambda_p = 1.064 \mu\text{m}$  with a repetition rate of 10 Hz and a pulse duration of 5.1 ns at  $1/e^2$  for PPKTP and 10 ns (FWHM) for 5%MgO:PPLN. The pump beam is properly focused in order to obtain parallel beam propagation inside the cylinder. The corresponding tuning curves are shown in Figure 14.

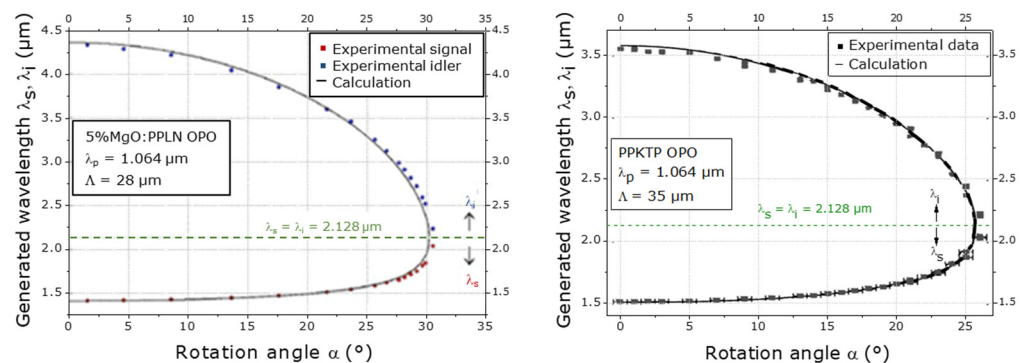


**Figure 14.** Tuning curves of AQPM OPO pumped at  $\lambda_p = 1.064 \mu\text{m}$ , giving the signal ( $\lambda_s$ ) and idler ( $\lambda_i$ ) wavelengths as a function of the rotation angle  $\alpha$  of the cylinders of 5%MgO:PPLN (left) and PPKTP (right).

In the case of PPKTP, the wavelength was tuned from 1.52  $\mu\text{m}$  to 3.56  $\mu\text{m}$ ; the maximum value of energy conversion efficiency was 17.3%, which corresponded to pump energy of 0.43 mJ, i.e., 3.5 times above the threshold [29]. For 5%MgO:PPLN, the tunability ranged between 1.41  $\mu\text{m}$  and 4.30  $\mu\text{m}$ , with an energy conversion efficiency of 27% when the crystal was pumped at 5 mJ, which was about five times above the threshold [30]. These energetical performances are similar to those of a classical OPO based on translated multi-grating periodically poled crystals [6]. However, in the case of AQPM implemented in cylinders, the tunability is continuous and does not require additional thermal tuning, which is a true advantage.

## 6. Conclusions

In conclusion, we provided a comprehensive description of both AQPM theory and experimental demonstrations over the two last decades in the cases of uniaxial and biaxial crystals. Benefits of AQPM are highlighted, which include: the extension of spectral ranges of solutions, the full consideration of all the possible polarization types; the full access to new directions of propagation that allow efficient nonlinear frequency conversion; the access to remarkable directions associated with giant spectral acceptances possibly more than two orders of magnitude larger than that in usual configuration soliciting the nonlinear coefficient  $\chi_{zzz}^{(2)}$  of ferroelectric crystals; the ability to tailor interactions by engineering the nonlinear grating period. We have also extended the AQPM approach in terms of scheme-A and scheme-B solutions, namely corresponding to positive and negative first-order AQPM solutions, respectively, which we presented here in a unified description. Therefore, AQPM provides a very rich space of solutions that encompasses that of BPM solutions, as detailed

by means of symmetry and topology of the associated cones. Such diversity results from the full investigation of the concomitant angular dependence of birefringence and of the effective periodical poling.

From a metrological and applicative point of view, this work provides a new vision that should help for the full characterization of high-interest periodically poled materials, especially PPLN and PPKTP and both isotypes [31]: new configurations that are associated with good nonlinear efficiencies and large spectral tolerances for the chosen material can then be identified. Such a determination is of prime importance while considering parametric processes achieved in the femtosecond regime, i.e., for efficient optical parametric chirped pulse amplification, for which some large spectral ranges need to be simultaneously frequency-converted so as to keep the ultrashort temporal pulse behavior for the generated beams [31,32].

Finally, the AQPM approach should be further extended in the future to other known uniaxial periodically poled crystals, such as PPLT [32] or periodically twinned Quartz [33]. Moreover, AQPM can also be applied to crystals belonging to the isotropic optical class, i.e., the cubic crystals such as orientation-patterned GaAs (OP-GaAs) [32–35] and or OP-ZnSe [36]. AQPM may also be relevant for photonic crystals [37–39], thermally poled micro-structured thin films [40], laser-structured glassy [41] or crystalline [42–45] materials to address nonlinear gratings bearing 3D periodicities. Therefore, AQPM should further stimulate the current effort on crystal growth, nonlinear material micro-structuring by electric or laser poling, as well as on developments in nonlinear nanophotonics [46].

**Author Contributions:** Conceptualization, B.B. and Y.P.; methodology, B.B., P.S. and Y.P.; experimental validation, P.S., A.P., S.J., D.L., Y.P. and B.B.; formal analysis, Y.P. and B.B.; writing—original draft preparation, Y.P. and B.B. with the help of A.P., S.J. and P.S.; writing—review and editing, Y.P., B.B., A.P., S.J., P.S. and D.L. All authors have read and agreed to the published version of the manuscript.

**Funding:** This research has benefited financial support from French National Research Agency (ANR) ANR-19-CE08-0021-01, and from Région Nouvelle Aquitaine (project AAPR2020-2019-8193110).

**Institutional Review Board Statement:** Not applicable.

**Informed Consent Statement:** Not applicable.

**Data Availability Statement:** Data underlying the results presented in this paper are not publicly available at this time but may be obtained from the authors upon reasonable request.

**Acknowledgments:** The authors wish to thank the following colleagues very much for the review made in Section 5 on previous experiments: Jérôme Debray, Bertrand Ménaert and David Jegouso from Institut Néel in France for the cutting of spheres and cylinders and help for the running of laser sources, Takunori Taira and Hideki Ishizuki from IMS in Japan for providing 5%MgO:PPLN samples and Carlota, Valdas Pasiskevicius and Fredrik Laurell from KTH in Sweden for providing PPRKTP samples.

**Conflicts of Interest:** The authors declare no conflict of interest.

## References

1. Franken, P.A.; Hill, A.E.; Peters, C.W.; Weinreich, G. Generation of optical harmonics. *Phys. Rev. Lett.* **1961**, *7*, 118. [[CrossRef](#)]
2. Armstrong, J.A.; Bloembergen, N.; Ducuing, J.; Pershan, P.S. Interactions between Light Waves in a Nonlinear Dielectric. *Phys. Rev.* **1962**, *127*, 1918. [[CrossRef](#)]
3. Hobden, M.V. Phase-matched second-harmonic generation in biaxial crystals. *J. Appl. Phys.* **1967**, *38*, 4365. [[CrossRef](#)]
4. Fève, J.; Boulanger, B.; Marnier, G. Calculation and classification of the direction loci for collinear types I, II and III phase-matching of three-wave nonlinear optical parametric interactions in uniaxial and biaxial acentric crystals. *Opt. Commun.* **1993**, *99*, 284. [[CrossRef](#)]
5. Stepanov, D.Y.; Shigorin, V.D.; Shipulo, G.P. Phase matching directions in optical mixing in biaxial crystals having quadratic susceptibility. *Sov. J. Quantum Electron.* **1984**, *14*, 1315. [[CrossRef](#)]
6. Fejer, M.; Magel, G.; Jundt, D.; Byer, R. Quasi-phase-matched second harmonic generation: Tuning and tolerances. *IEEE J. Quantum Electron.* **1992**, *28*, 2631. [[CrossRef](#)]

7. Eyres, L.A.; Tourreau, P.J.; Pinguet, T.J.; Ebert, C.B.; Harris, J.S.; Fejer, M.M.; Becouarn, L.; Gerard, B.; Lallier, E. All-epitaxial fabrication of thick, orientation-patterned GaAs films for nonlinear optical frequency conversion. *Appl. Phys. Lett.* **2001**, *79*, 904. [CrossRef]
8. Haïdar, R.; Forget, N.; Kupecek, P.; Rosencher, E. Fresnel phase matching for three-wave mixing in isotropic semiconductors. *J. Opt. Soc. Am. B* **2004**, *21*, 1522. [CrossRef]
9. Fiore, A.; Berger, V.; Rosencher, E.; Bravetti, P.; Nagle, J. Phase matching using an isotropic nonlinear optical material. *Nature* **1998**, *391*, 463. [CrossRef]
10. Rosencher, E.; Winter, B. *Optoelectronics*; Cambridge University Press: Cambridge, UK, 2002.
11. Fève, J.-P.; Pacaud, O.; Boulanger, B.; Ménaert, B.; Hellström, J.; Pasiskevicius, V.; Laurell, F. Widely and continuously tunable optical parametric oscillator based on a cylindrical periodically poled KTiOPO<sub>4</sub> crystal. *Opt. Lett.* **2001**, *26*, 1882–1884. [CrossRef]
12. Fève, J.-P.; Boulanger, B.; Ménaert, B.; Pacaud, O. Continuous tuning of a microlaser-pumped optical parametric generator by use of a cylindrical periodically poled lithium niobate crystal. *Opt. Lett.* **2003**, *28*, 1028. [CrossRef]
13. Ishizuki, H.; Shoji, I.; Taira, T. Periodical poling characteristics of congruent MgO:LiNbO<sub>3</sub> crystals at elevated temperature. *Appl. Phys. Lett.* **2003**, *82*, 4062. [CrossRef]
14. Zukauskas, A.; Thilmann, N.; Pasiskevicius, V.; Laurell, F.; Canalias, C. 5 mm thick periodically poled Rb-doped KTP for high energy optical parametric frequency conversion. *Opt. Mater. Express* **2011**, *1*, 201. [CrossRef]
15. Petit, Y.; Boulanger, B.; Segonds, P.; Taira, T. Angular quasi-phase-matching. *Phys. Rev. A* **2007**, *76*, 063817. [CrossRef]
16. Brand, P.; Boulanger, B.; Segonds, P.; Petit, Y.; Félix, C.; Ménaert, B.; Taira, T.; Ishizuki, H. Angular quasi-phase-matching: Theory and first experiments. *Proc. SPIE* **2009**, *7197*, 719706.
17. Brand, P.; Boulanger, B.; Segonds, P.; Petit, Y.; Félix, C.; Ménaert, B.; Taira, T.; Ishizuki, H. Angular quasi-phase-matching experiments and determination of accurate Sellmeier equations for 5%MgO:PPLN. *Opt. Lett.* **2009**, *34*, 2578–2580. [CrossRef]
18. Petit, Y.; Brand, P.; Boulanger, B.; Segonds, P. Classification of angular quasi-phase matching loci in periodically poled uniaxial crystals. *Opt. Mater.* **2010**, *32*, 1501–1507. [CrossRef]
19. Hum, D.S.; Route, R.K.; Fejer, M.M. Quasi-phase-matched second-harmonic generation of 532 nm radiation in 25°-rotated, x-cut, near-stoichiometric, lithium tantalate fabricated by vapor transport equilibration. *Opt. Lett.* **2007**, *32*, 961–963. [CrossRef]
20. Lu, D.; Peña, A.; Segonds, P.; Debray, J.; Joly, S.; Zukauskas, A.; Laurell, F.; Pasiskevicius, V.; Yu, H.; Zhang, H.; et al. Validation of the angular quasi-phase-matching theory for the biaxial optical class using PPRKTP. *Opt. Lett.* **2018**, *43*, 4276. [CrossRef]
21. Petit, Y.; Peña, A.; Segonds, P.; Debray, J.; Joly, S.; Zukauskas, A.; Laurell, F.; Pasiskevicius, V.; Canalias, C.; Boulanger, B. Demonstration of Negative First-Order Quasi-Phase Matching in a periodically-poled Rb-doped KTiOPO<sub>4</sub> crystal. *Opt. Lett.* **2020**, *45*, 6026–6029. [CrossRef]
22. Yariv, A.; Yeh, P. *Optical Waves in Crystals*; Wiley: New York, NY, USA, 2002.
23. Boulanger, B.; Zyss, J.J. Non-linear Optical properties, Chapter 1.7. In *International Tables for Crystallography, Vol. D: Physical Properties of Crystals*; Authier, A., Ed.; International Union of Crystallography, Kluwer Academic Publisher: Dordrecht, The Netherlands, 2013; pp. 181–222.
24. Yao, J.Q.; Fahlen, T.S. Calculations of optimum phase match parameters for the biaxial crystal KTiOPO<sub>4</sub>. *J. Appl. Phys.* **1984**, *55*, 65. [CrossRef]
25. Boulanger, B.; Segonds, P.; Ménaert, B.; Zaccaro, J. Spheres and cylinders in nonlinear optics. *Opt. Mat.* **2004**, *26*, 459–464. [CrossRef]
26. Ménaert, B.; Debray, J.; Zaccaro, J.; Segonds, P.; Boulanger, B. Cutting and polishing bulk cylinders and spheres for linear and nonlinear optics. *Opt. Mat. Express* **2017**, *7*, 3017–3022. [CrossRef]
27. Boulanger, B.; Fève, J.P.; Marnier, G.; Bonnin, C.; Villeval, P.; Zondy, J.J. Absolute measurement of quadratic nonlinearities from phase-matched second-harmonic generation in a single KTP crystal cut as a sphere. *J. Opt. Soc. Am. B* **1997**, *14*, 1380–1386. [CrossRef]
28. CASIX Company. LiNbO<sub>3</sub> Crystal Series. Available online: <https://www.casix.com/products/crystal-products/non-linear-optical-crystals/linb03-crystal.shtml> (accessed on 1 February 2022).
29. Fève, J.P.; Pacaud, O.; Boulanger, B.; Ménaert, B.; Hellström, J.; Laurell, F. Widely and continuously tunable quasi-phase-matched OPO using a cylindrical ppKTP crystal. In Proceedings of the CLEO'01-Conference on Lasers and Electro-Optics, PDP, Baltimore, MD, USA, 6–11 May 2001.
30. Kemlin, V.; Jegouso, D.; Debray, J.; Segonds, P.; Boulanger, B.; Ménaert, B.; Ishizuki, H.; Taira, T. Widely tunable Optical Parametric Oscillator in a 5 mm-thick 5%MgO:PPLN partial cylinder. *Opt. Lett.* **2013**, *38*, 860–862. [CrossRef]
31. Karlsson, H.; Laurell, F. Electric field poling of flux grown KTiOPO<sub>4</sub>. *Appl. Phys. Lett.* **1997**, *71*, 3474. [CrossRef]
32. Rotermund, F.; Yoon, C.J.; Petrov, V.; Noack, F.; Kurimura, S.; Yu, N.-E.; Kitamura, K. Application of periodically poled stoichiometric LiTaO<sub>3</sub> for efficient optical parametric chirped pulse amplification at 1 kHz. *Opt. Express* **2004**, *12*, 6421–6427. [CrossRef]
33. Kurimura, S.; Harada, M.; Muramatsu, K.-I.; Ueda, M.; Adachi, M.; Yamada, T.; Ueno, T. Quartz revisits nonlinear optics: Twinned crystal for quasi-phase matching [Invited]. *Opt. Mater. Express* **2011**, *1*, 1367–1375. [CrossRef]
34. Tanimoto, R.; Takahashi, Y.; Shoji, I. Quasi-phase-matching stack of 25 GaAs plates with high transmittance for high-power mid-infrared wavelength conversion fabricated by use of room-temperature bonding. *J. Opt. Soc. Am. B* **2021**, *38*, B30. [CrossRef]

35. Vodopyanov, K.L.; Sorokin, E.; Sorokina, I.T.; Schunemann, P.G. Mid-IR frequency comb source spanning 4.4–5.4  $\mu\text{m}$  based on subharmonic GaAs optical parametric oscillator. *Opt. Lett.* **2011**, *36*, 2275–2277. [[CrossRef](#)]
36. Mustelier, A.; Rosencher, E.; Kupecek, K.; Godard, A.; Baudrier, M.; Lefèbvre, M.; Poulat, M.; Mennerat, G.; Pasquer, C.; Lemasson, P. Mid-IR difference frequency generation in quasi-phase matched diffusion bonded ZnSe plates. *Appl. Phys. Lett.* **2004**, *84*, 4424. [[CrossRef](#)]
37. Berger, V. Nonlinear photonic crystals. *Phys. Rev. Lett.* **1998**, *81*, 4136. [[CrossRef](#)]
38. Lifshitz, R.; Arie, A.; Bahabad, A. Photonic quasi-crystals for nonlinear optical frequency conversion. *Phys. Rev. Lett.* **2005**, *95*, 133901. [[CrossRef](#)]
39. Ousaid, S.M.; Chakaroun, M.; Chang, K.-H.; Billeton, T.; Peng, L.-H.; Boudrioua, A. Multi-resonant optical parametric oscillator without mirrors based on 1D and 2D-PPLT nonlinear photonic crystal. *EPJ Web Conf.* **2020**, *238*, 11003. [[CrossRef](#)]
40. Karam, L.; Adamietz, F.; Michau, D.; Gonçalves, C.; Kang, M.; Sharma, R.; Murugan, G.S.; Cardinal, T.; Fargin, E.; Rodriguez, V.; et al. Electrically Micro-Polarized Amorphous Sodo-Niobate Film Competing with Crystalline Lithium Niobate Second-Order Optical Response. *Adv. Opt. Mater.* **2020**, *8*, 2000202. [[CrossRef](#)]
41. Papon, G.; Marquestaut, N.; Petit, Y.; Royon, A.; Dussauze, M.; Rodriguez, V.; Cardinal, T.; Canioni, L. Femtosecond direct laser poling of sub-micron, stable and efficient second-order optical properties in a tailored silver phosphate glass. *J. Appl. Phys.* **2014**, *115*, 113103. [[CrossRef](#)]
42. Thomas, J.; Hilbert, V.; Geiss, R.; Pertsch, T.; Tunnermann, A.; Nolte, S. Quasi-phase-matching in femtosecond pulse volume structured x-cut lithium niobate. *Laser Photonics Rev.* **2013**, *7*, 17–20. [[CrossRef](#)]
43. Wei, D.; Wang, C.; Wang, H.; Hu, X.; Wei, D.; Fang, X.; Zhang, Y.; Wu, D.; Hu, Y.; Li, J.; et al. Experimental demonstration of a three-dimensional lithium niobate nonlinear photonic crystal. *Nat. Photonics* **2018**, *12*, 596–600. [[CrossRef](#)]
44. Xu, T.; Świtkowski, K.; Chen, X.; Liu, S.; Koynov, K.; Yu, H.; Zhang, H.; Wang, J.; Sheng, Y.; Krolikowski, W. Three-dimensional nonlinear photonic crystal in ferroelectric barium calcium titanate. *Nat. Photonics* **2018**, *12*, 591–595. [[CrossRef](#)]
45. Shao, M.; Liang, F.; Yu, H.; Zhang, H. Angular engineering strategy of an additional periodic phase for widely tunable phase-matched deep-ultraviolet second harmonic generation. *Light. Sci. Appl.* **2022**, *11*, 31. [[CrossRef](#)] [[PubMed](#)]
46. Ledezma, L.; Sekine, R.; Guo, Q.; Nehra, R.; Jahani, S.; Marandi, A. Intense optical parametric amplification in dispersion-engineered nanophotonic lithium niobate waveguides. *Optica* **2022**, *9*, 303. [[CrossRef](#)]